ISSN 1063-4576, Journal of Superhard Materials, 2015, Vol. 37, No. 2, pp. 101–111. © Allerton Press, Inc., 2015.
Original Russian Text © A.D. Pogrebnjak, B.A. Postol'nyi, Yu.A. Kravchenko, A.P. Shipilenko, O.V. Sobol', V.M. Beresnev, A.P. Kuz'menko, 2015, published in Sverkhtverdye Materialy, 2015, Vol. 37, No. 2, pp. 46–59.

PRODUCTION, STRUCTURE, PROPERTIES

Structure and Properties of (Zr–Ti–Cr–Nb)N Multielement Superhard Coatings

A. D. Pogrebnjak[a, *], B. A. Postol'nyi[a], Yu. A. Kravchenko[a], A. P. Shipilenko[a], O. V. Sobol'[b], V. M. Beresnev[c], and A. P. Kuz'menko[d]

[a] *Sumy State University, vul. Rimskogo-Korsakova 2, Sumy, 40007 Ukraine*
[b] *National Technical University Kharkiv Polytechnic Institute, vul. Frunze 21, 61002 Kharkiv, Ukraine*
[c] *Karazin Kharkiv National University, sq. Peremogy 4, Kharkiv, 61022 Ukraine*
[d] *Southwest State University, ul. 50 let Oktyabrya 94, Kursk, Russia*
**e-mail: alexp@i.ua*

Received June 3, 2014

Abstract—Structure and properties of (Zr–Ti–Cr–Nb)N multicomponent nanostructured coatings fabricated by a vacuum-arc deposition have been investigated. It has been found that the coatings thickness attained 6.2 μm, hardness and indentation load that is responsible for the stress exceeding cohesion strength of coatings were $H = 43.7$ GPa and $L_c = 62.06$ N, respectively. In coatings structures have been identified that consist of three interstitial phases having cubic, hexagonal, and tetragonal lattices. The nanocrystallites sizes were from 4 to 7.3 nm. The results of the SEM, TEM, EDS, and XRD analysis have been also considered.

DOI: 10.3103/S1063457615020045

Keywords: multielement coatings, nitrides, vacuum-arc evaporation, phase and elemental compositions, microhardness, cohesion, strength.

1. THE URGENCY OF THE PROBLEM

The increasing service life of industrial equipments, components of plants, machines, cutting, drilling, and other machining tools has always been the important problem of science and engineering. In the course of the enhanced saving of resources and conversion to energy-saving technologies this question becomes especially interesting. During the operation of the above products the surface layers of them are subjected to the highest load, physico-mechanical, chemical, and thermal actions. One of the methods to protect and improve various surface properties is the surface modification by the formation of coatings from nanostructured materials. Small (below 10 nm) grain sizes of such materials and a considerable increasing of a volume content of interfaces allows one to achieve the unique properties (hardness, plasticity, wear, high temperatures, and corrosion resistance) [1–6]. The coating deposition by a vacuum-arc discharge makes it possible to introduce the results of studies into the manufacture of products of various functionalities [7–10].

Recently nanostructural coatings of complex elemental and phase compositions have aroused considerable interest, as the combinations of different elements make it possible to use the best properties of two or several metals and nitrides of them [11, 12]. For example, zirconium is the basic component of constructional alloys for nuclear engineering. It has a small section of a thermal neutron capture and high melting temperature ($T_{melt} = 1852$°C). Zr is refractory and highly plastic but its strength at both dynamic and static loads is low [6, 13]. The alloying zirconium with niobium, iron, and aluminum facilitates increase of the material plasticity [14]. An introduction of niobium, silicon, and titanium atoms into Zr results in an increase of the chemical stability of the system [15, 16], etc. Therefore, the problem of increasing the surface mechanical characteristics by the formation of nanostructural multilayer [17–20] and multicomponent [9, 13, 16, 21] coatings of carbides, nitrides, borides, and silicides of transition metals is profitable from the practical point of view.

2. STATE OF THE ART

Coatings of titanium nitrides, carbides, and carbonitrides 5–10 μm thick are the best understood and widely used. However, the possibilities to increase hardness and plasticity of the surface layer in the deposition of simple nitrides are virtually exhausted as already at temperatures of 400–500°C titanium carbides and nitrides are thermally unstable.

In the last years particular attention has been given to the development of superhard nanostructural coatings that are produced using three– (Ti–Nb–N, Ti–Cr–N, Zr–Ti–N) [4, 11, 12, 17], four–(Zr–Ti–Si–N) [16, 18] or five– (Zr–Nb–Ti–Cr–N) component systems [19, 22]. The structures and properties as well as the possibilities of thermal stabilization of the phase compositions of such alloyed condensates are poorly known for the present. But as a whole the above materials exhibit a higher hardness (up to 36–50 GPa) [5, 6, 8, 17], elasticity (300–425 GPa) [3, 8], and thermal stability [5]. Among these studies the research of Taiwan scientists [19] stands out, where the five-component coatings (Zr–Ti–Cr–Nb)N exhibits a low hardness (2.5 GPa) and Young modulus (93 GPa), which is even below the values of the ZrTiCrNb ($H = 4.7$ GPa) target produced by arc melting according to the authors version. One of the reasons for such a softness of the material is probably a high nitrogen concentration (about 47 at % at a flow of 8 cm^3/min). However, this interpretation of the results leaves something to be discussed, as the nitrogen concentration is sufficient for the formation of a harder material [8, 22–27]. A complex of physical and mechanical properties of pure metals like zirconium, niobium, titanium, molybdenum, and chromium, allows us to assume that the investigation of vacuum–plasma condensates based on the Zr–Ti–Cr–Nb system is advisable. This in turn allows one to generate a protecting layer (or coating) of five elements (four transition metals and nitrogen as a bonding agent).

The aim of our investigation was to study the effect of the parameters of the deposition of nanostructural coatings (Zr–Ti–Cr–Nb)N on the elemental and phase compositions of the protecting layer and its mechanical characteristics.

3. MATERIALS AND RESEARCH PROCEDURE

Protective coatings about 6.2 μm thick were deposited onto polished substrates surfaces (the materials were steel of the 45 grade, silicon) in a molecular nitrogen atmosphere using a Bulat-6 vacuum-arc plant. The evaporable material was a one-piece cathode Zr + Ti + Cr + Nb (having the composition Cr—37.39, Zr—27.99, Nb—22.30, Ti—12.32 at %) produced by electron–beam melting. Table 1 shows physico-technological parameters of the deposition of the (Zr–Ti–Cr–Nb)N coatings. The use of the pulse stimulation in the formation of series 5 coatings makes possible the intensification of the ion–plasma flow energy, which improves the film adhesion to the substrate and provides a possibility of producing more disperse coating structure.

Table 1. Deposition parameters of (Zr–Ti–Cr–Nb)N coatings

Series	Evaporant	I_a, A	p, Pa	U_b, V
1	Zr, Ti, Cr, Nb	110	0.3	–100
2			0.7	–100
3			0.3	–200
4			0.7	–200
5*			0.7	–200

*Pulse stimulation was used.

The morphology of the coatings surfaces was studied using JEOL JSM-6610 LV and FEI Quanta 600 FEG scanning electron microscopes and an atomic force microscope on a platform of the AIST-NT SmartSPM company. The elemental analysis of the coating surface was made using an X-Max Silicon Drift Detector energy dispersive analyzer built into the JEOL JSM-6610 LV scanning electron microscope. The sensor design offers a high effectiveness at a very low energy (the resolution is 125 eV). The structure and phase composition of the coating material were analyzed by XRD method (D8 ADVANCE and DRON-4) in the Cu$K\alpha$ radiation. The direct studies of the structures of the (Zr–Ti–Cr–Nb)N resultant coatings were conducted using a JEOL JEM-2100 transmission electron microscope.

The coatings microhardness was measured by the Vickers method using an AFFRI DM-8 automated hardness tester. The imprints were spaced at intervals of 1.0 mm. We made 10 measurements for each sample. Before the measurements the coatings were polished in order to eliminate the effects of a drop component and surface roughness on the measurement accuracy.

To assess the cohesion strength we used a REVETEST (CSM Instruments) scratch tester. The scratches were made on coatings at a constant increasing of the load on a Rockwell C spherical diamond indenter with a radius of a curvature of 200 mm. The registered parameters were: acoustic emission, friction coefficient and depth of the indenter penetration. We fixed the following basic loads from the variations of curves of the friction coefficient and acoustic emission dependences on scribing loads: L_{c1} characterizes the instant of the

appearance of the first chevron crack; L_{c2}—the moment of the appearance of chevron cracks; L_{c3} indicates the fracture of a cohesion-adhesion mode, L_{c4}—a local delamination of coating regions, L_{c5}—plastic abrasion of the coating up to the substrate.

4. RESULTS AND DISCUSSION

According to the results of scanning electron microscopy, the vacuum–arc condensation of a multicomponent system has a number of peculiarities in the formation of the surface morphology. Figure 1a shows a SEM image of one of the coatings produced (series 1). The basis of its matrix consists of cells similar to cells on the surface of vacuum–arc coatings produced of nitrides of refractory elements. In addition, the coating contains also rounded inclusions of a drop fraction up to 6 μm in diameter. An increase of the nitrogen pressure to 0.7 Pa in the course of the deposition does not produce particular changes into the surface morphology, while an increase of the temperature of the deposition flow using a bias voltage ($U_b = -200$ V) considerably decreases a drop fraction concentration on the surface (see Fig. 1b). Probably the focusing of a beam of charged particles activates the process of cleaning the surface from smaller fractions and its heating allows the formation of a uniform protecting layer.

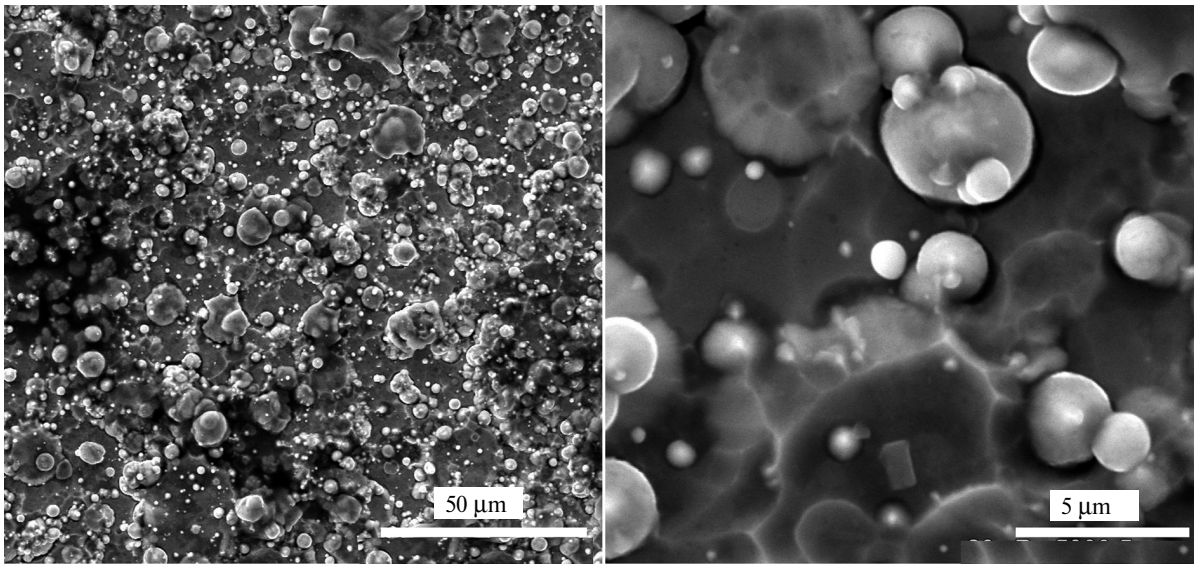

(a)

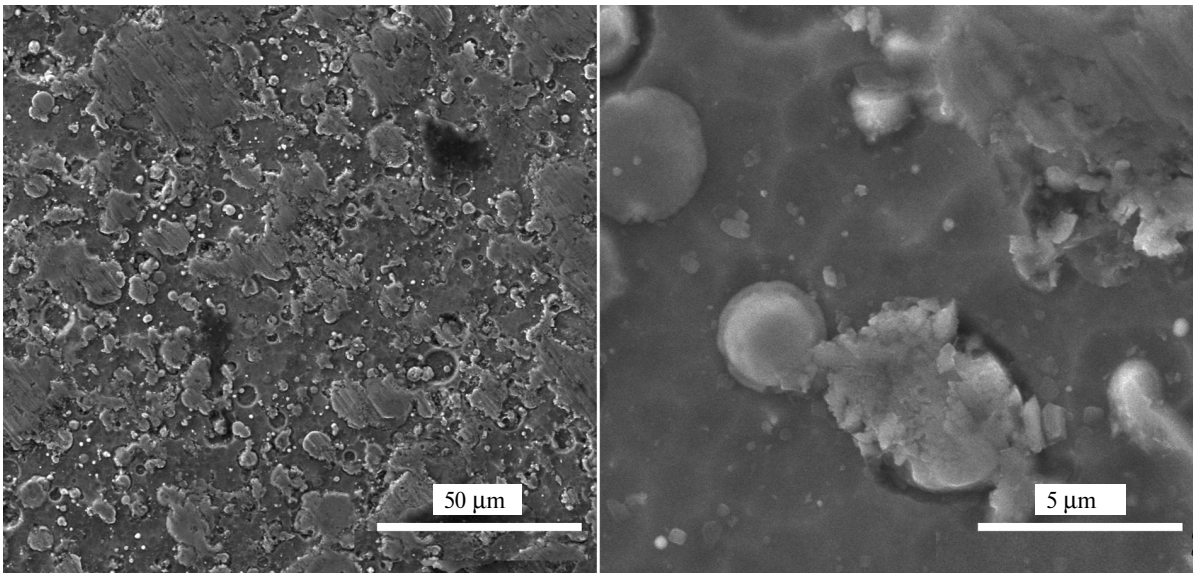

(b)

Fig. 1. SEM images of coatings of series 1 (a) and 4 (b).

The integral elemental analysis showed that Zr, Ti, Cr, and Nb composed the matrix of the coating near-surface region (Fig. 2, Table 2). The presence of nitrogen peaks in spectra is caused by the composition of the gas atmosphere of a vacuum–arc source.

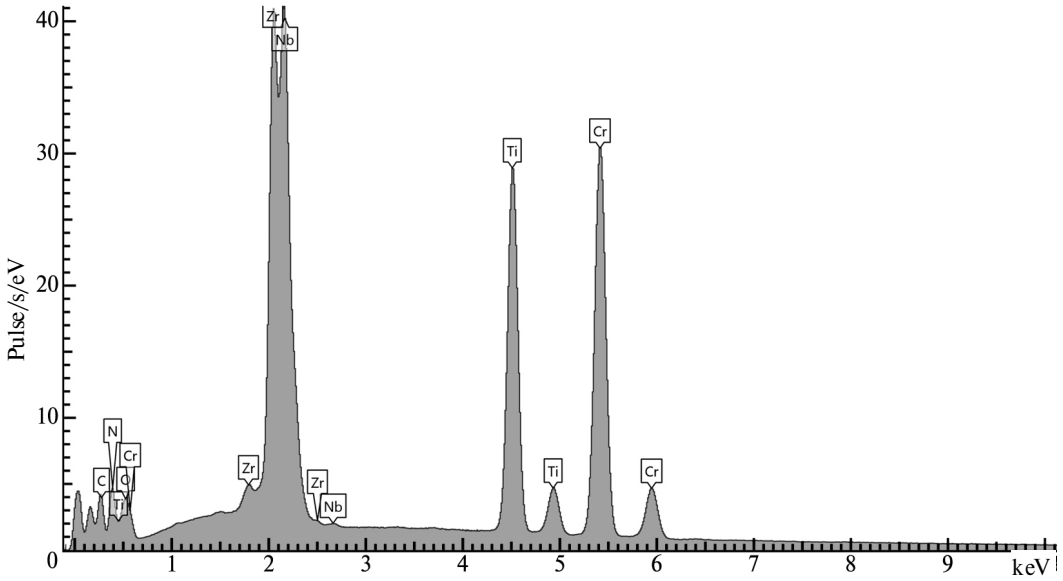

Fig. 2. Integral elemental composition of the (Zr–Ti–Cr–Nb)N coating.

Table 2. Elemental analysis of the (Zr–Ti–Cr–Nb)N coatings

Series	Concentration, at %							
	Ti	Zr	Cr	Nb	N	C	O	Impurities
1	10.21	6.63	15.22	4.96	18.70	38.29	5.42	0.57
2	12.30	8.48	16.92	6.17	22.32	27.35	6.46	–
3	11.27	8.03	18.23	7.48	23.20	31.79	–	–
4	10.40	7.81	11.00	6.73	22.66	35.63	5.37	0.39

A high carbon concentration on the sample surface may be explained by the complexity of the identification of elements like C, N, O by the energy dispersive X-ray spectrometry because of the similarity of their electron structures. By calculating energy E of the radiation $K\alpha$ for some elements, defining the difference between them and comparing with the resolution of the analyzer, one may make a conclusion about the accuracy of the obtained results. It follows from the Mosely law

$$E = 10.2eV \cdot (Z-1)^2 \quad (1)$$

$$\Delta E = 10.2eV \cdot \left((Z_A-1)^2 - (Z_B-1)^2\right) = 10.2eV \cdot (Z_A + Z_B - 2)(Z_A - Z_B), \quad (2)$$

where Z is an ordinal number of an atom in the Mendeleev periodic system of chemical elements.

According to the calculations, the difference between the radiation energies, ΔE, in the determination of the elements using EDS were 112.2 eV for C and N, 132.6 eV for N and O, and 805.8 eV for Zr and Nb. As the difference between the radiation energies of the C, N, and N, O elements is lower than the analyzer resolution, to accurately define the ratio between these elements in a coating is impossible. It is quite probable that oxygen in the coating is virtually absent and the diffusion of oxygen atoms into the surface composition from the air atmosphere may be the reason for its appearance in the spectrum. The nitrogen concentration should be somewhat higher due to a decrease of the carbon concentration.

On the basis of the nonuniform contrast of inclusions in the SEM images (see Fig. 1), drop fractions have elemental compositions different in stoichiometry. According to the maps of the elements distribution (Fig. 3), zirconium, niobium, and nitrogen are the basis of these inclusions. It should be noted that Nb and Zr virtually duplicate their locations in the map of elements and mainly compose the matrix of inclusions of drop

fractions. The reason for this distribution is a high melting temperature of both elements and virtually equal work of electrons liberation from the metal surface (A_{lib}(Nb) = 3.99 eV, A_{lib}(Zr) = 3.96–4.16 eV). According to the calculations, the difference between the radiation energies of zirconium and niobium is several times greater than the threshold of the resolution of the energy dispersive X-ray spectra analyzer, which allows the identification of the above elements. Therefore, the presence of the drop fractions of Nb and Zr is quite possible (bright balls in Fig. 1a).

Titanium and nitrogen exhibit a uniformly equal mode of the distribution over the whole coating surface (Fig. 3), while the chromium concentration is much lower in the regions, where niobium dominates. It is also seen that the C distribution repeats the N distribution not over the whole surface; hence, this is not a measurement error.

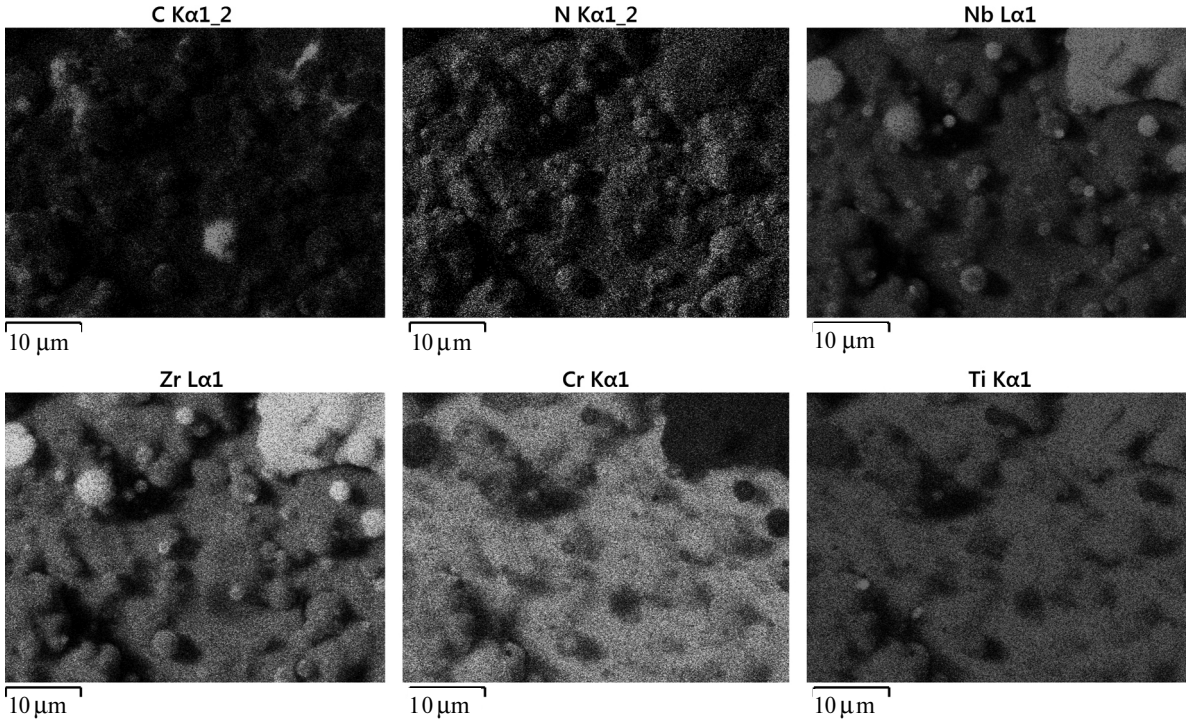

Fig. 3. Maps of the elements distribution over the surface of a series 1 sample.

In all produced coatings the pattern of the element distribution by concentration in the surface composition exhibits a similar regularity $C_C > C_N > C_{Cr} > C_{Ti} > C_{Zr} > C_{Nb.}$ This is clearly illustrated by circle diagrams shown in Fig. 4. It should be also noted that an increase of the bias voltage to –200 V results in a noticeable decrease of the titanium and chromium concentrations in the surface composition. It means that in the course of the coating deposition particles of the coating surface having the lowest atomic weight disperse.

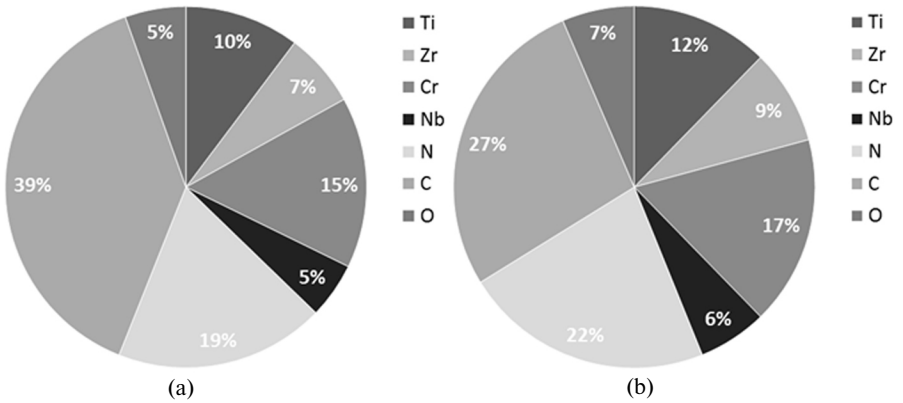

(a) (b)

Fig. 4. Elemental compositions of (Zr–Ti–Cr–Nb)N coatings: series 1 (a), 2 (b), 3 (c), 4 (d).

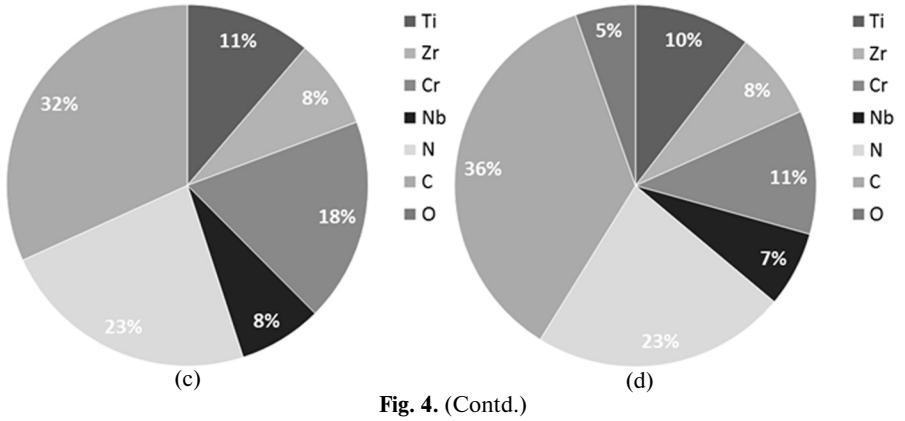

Fig. 4. (Contd.)

It is seen from the graphs shown in Fig. 5 that an increase of the nitrogen pressure in the chamber from 0.3 to 0.7 Pa results in the decrease of the carbon concentration in the surface composition and increase of the concentration of nitrogen, niobium, and zirconium atoms. The same thing was observed also as the substrate negative potential increases from −100 to −200 V.

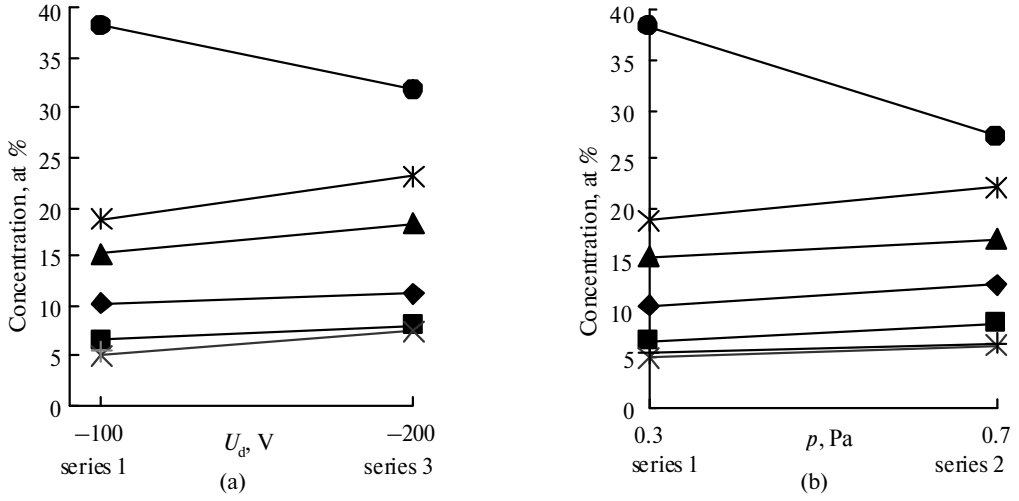

Fig. 5. Variation of the element concentration in the (Zr–Ti–Vr–Nb)N coatings depending on the substrate voltage at p = 0.3 Pa (a) and nitrogen pressure in the chamber, at U_b −100 V (b): Ti (◆), Zr (■), Cr (▲), Nb (×), N (∗), C (●), O (+).

The results of the electron microscopy and diffraction studies (Fig. 6) indicate that during the condensation of the Zr–Ti–Cr–Nb transition metals system there forms a coating with a fine-dispersed structure. In the electron–diffraction patterns one observes rings of the fcc phase. Taking into account the elemental composition, one may state that the revealed fcc phase is of the NaCl type and in its lattice points metal atoms of zirconium, chromium, titanium, and niobium are situated. This mixture of elements forms a solid solution, in octahedral interstices of which the N, O, C interstitial elements are located.

According to the results of the X-ray structure analysis (Fig. 7) the intermetallic compound Zr–Cr may be assigned to the basic phases of the coating composition. All diffraction maxima corresponding to the low-temperature β-$ZrCr_2$($P6_3/mmc$) phase with the lattice parameters a = 0.506 nm and c = 0.828 nm (a_{tabl} = 0.5089 nm, c_{tabl} = 0.8279 nm, 06-0613, DB PCDFWIN) are clearly shown in the X-ray patterns. Similar to the results of the electron microscopy in the X-ray radiation spectra the lines that correspond to the fcc lattice of the NaCl type are also seen.

Based on the analysis of the phase diagrams for the Ti–Zr–Cr–Nb–N system, one may assume that the Ti–Zr, Cr–Ti, and Cr–Nb solid solutions may be present in the coating composition [11]. The film deposition in the molecular nitrogen atmosphere and elemental analysis of the coatings surfaces imply the formation of nitride compounds (Ti, Cr, Nb, Zr)N.

The phase analysis indicates the presence of the TiN fcc phase (a = 0.243 nm, a_{tabl} = 0.244 nm [4, 20]) and Cr_2N tetragonal modification. As the chromium content of the coating increases, in diffraction spectra the

diffraction maxima of the Cr_2N-type tetragonal phase (trigonal lattice (space group $P31m$), parameters a = 0.4800 nm and c = 0.4472 nm [26]) with a higher period increase because of an increased nitrogen content (compare spectra 1–2 and 3–4 in Fig. 7).

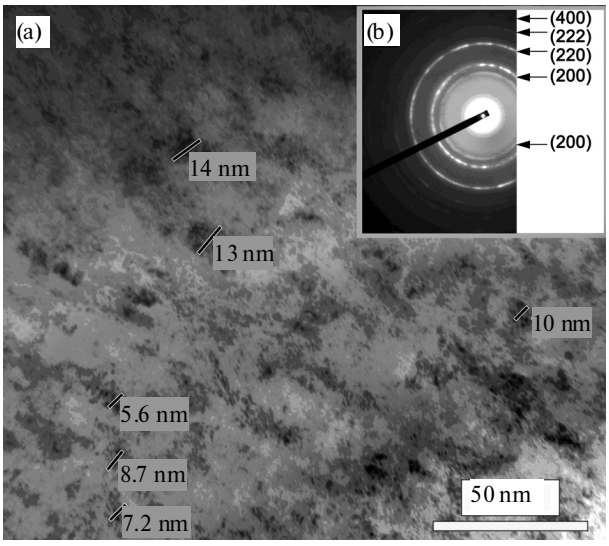

Fig. 6. Image of the (Zr–Ti–Vr–Nb)N coating produced using electron microscopy: bright-field image (a), microdiffraction picture (b).

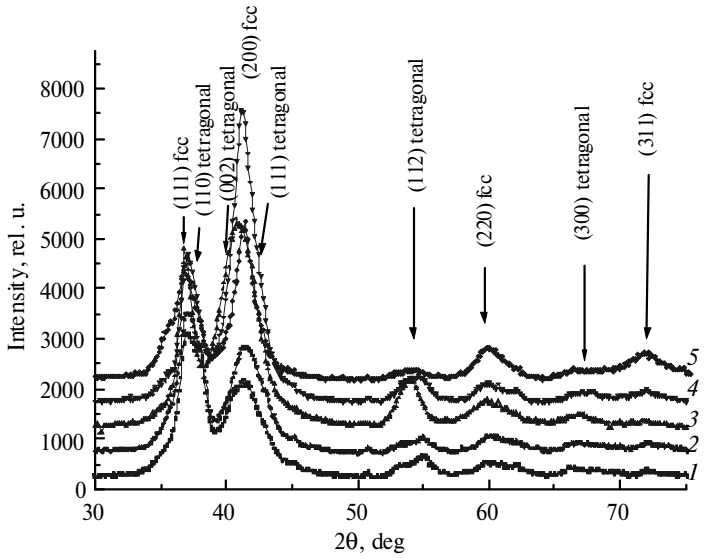

Fig. 7. X-ray radiation spectra from samples of 1–5 series: 1 (*1*), 2 (*2*), 3 (*3*), 4 (*4*), 5 (*5*).

The crystal sizes, L_{hkl} were calculated by the procedure allowing for the broadening of diffraction maxima [19], according to which

$$L_{hkl} = \frac{\beta \cos\theta}{\xi\lambda}, \tag{3}$$

where L_{hkl} is the mean size of crystals normally to the reflecting surface, β is the peak physical broadening, λ is the length of the X-ray radiation wave = 1.54 Å, θ is the Bragg angle, corresponding to the diffraction maximum chosen for calculations, ξ is the multiplier that allows for the indices of the reflecting plane.

Period and sizes of regions of ordering (crystallites) found for crystals with the fcc lattice are given in Table 3.

Table 3. Size of crystallites, L, and lattice constant of the phase with the fcc lattice

Parameter	Series				
	1	2	3	4	5
L, nm	5.2	4.5	5.1	6.9	7.3
Lattice constant, nm	0.4365	0.4359	0.441	0.4381	0.4371

Thus, in the course of the deposition there forms a three-phase structure of the interstitial phases with cubic, hexagonal, and tetragonal crystal lattices. The crystallites size in the more complex tetragonal lattice defined for samples of series 3 and 4 made ~ 5 nm.

According to the tabulated data, microhardnesses of nitrides of the materials used to form coatings are, respectively, $H_\mu(\text{TiN}) = 20$, $H_\mu(\text{ZrN}) = 16$, $H_\mu(\text{NbN}) = 14$, $H_\mu(\text{Cr}_2\text{N}) = 15.7$ GPa [25]. A combined use of transition metals nitrides allows to make a protecting layer, whose microhardness is higher by a factor of 2.2–2.5. The results of the measurements for the (Zr + Ti + Cr + Nb)N coatings are shown in Fig. 8. An increase of the microhardness is observed for coatings with larger crystallites produced at the increased (up to 0.7 Pa) nitrogen pressure, increased (to –200 V) bias voltage, and the use of the pulse stimulation.

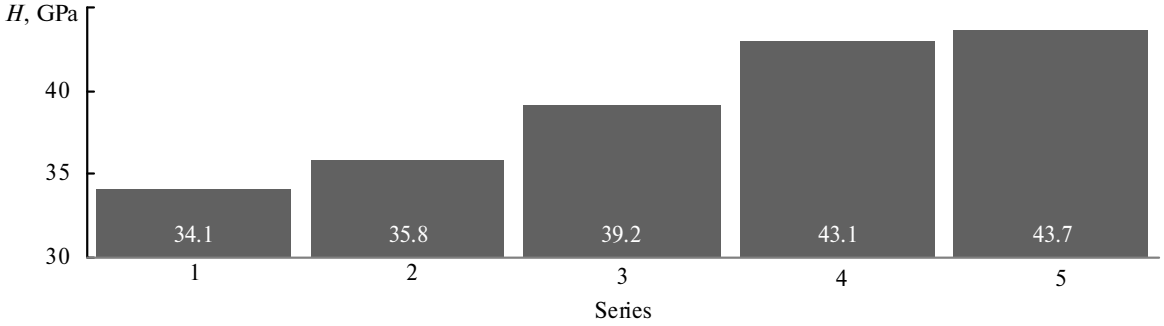

Fig. 8. Results of the (Zr–Ti–Vr–Nb)N coatings microhardness measurements.

The results of adhesion tests of coatings are shown as a histogram in Fig. 9. To obtain reliable results, we made two scratches on the surface of samples with coatings. For comparison we used samples with vacuum-arc deposited coatings based on TiN with hardness $H = 28.0$ GPa.

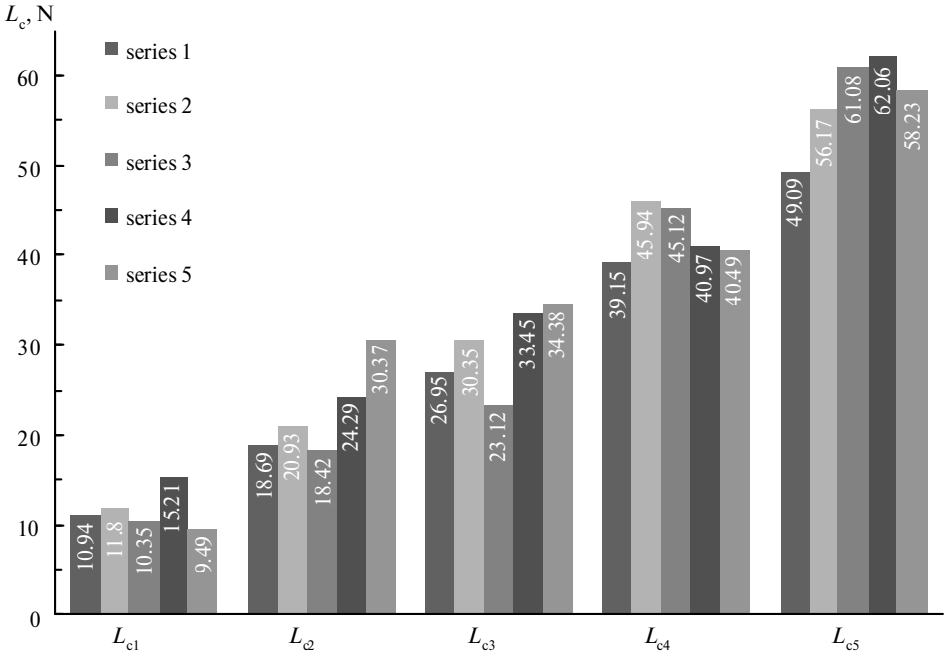

Fig. 9. Results of the adhesion tests of the (Zr–Ti–Vr–Nb)N coatings.

Figure 10 shows the curve of the friction coefficient, μ, variation during a displacement of a diamond indenter over the surface of a (Zr–Ti–Cr–Nb)N coating (sample 4) and the curve of variation of the acoustic emission signal (AE). As is seen from the data obtained, the process of a coating fracture in scratching by diamond indenter may be divided into several stages. At first the indenter monotonically penetrates into the coating and first cracks appear (the load up to 15.21 N), friction coefficient μ increases and the acoustic emission signal increases slightly. Then as the load increases, shevron and diagonal cracks appear [1, 10], which results in an increase of the friction coefficient to 0.3. At the load above 14 N the level of the signal amplitude abruptly increases and the AE value remains approximately at the same level to the end of the test. Later as the load increases attaining 62 N, the coating local abrasion takes place up to the substrate material (Fig. 11).

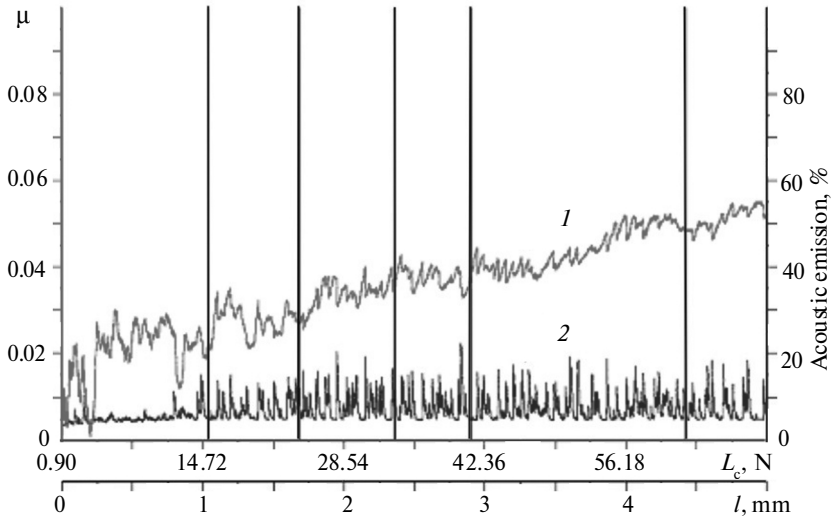

Fig. 10. Dependence of the friction coefficient (*1*) and acoustic emission (*2*) on L_c load and the length of the scribing way, *l*, for a sample of series 4.

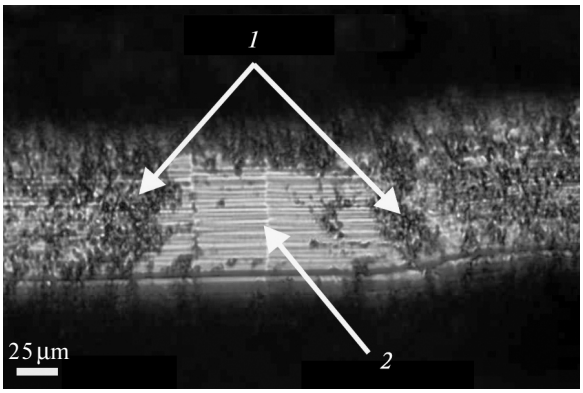

Fig. 11. Image of a scratch after the indenter action: coating (*1*), substrate (*2*).

The comparative analysis testifies that in scratching coatings wear but do not delaminate, i.e., the cohesion fracture takes place, which is caused by the plastic deformation and formation of fatigue cracks in the coating material.

The measurements show that the indentation load caused the stresses exceeding the cohesion strength of a (Zr–Ti–Cr–Nb)N multicomponent coating is $L_c = 62.06$ N.

5. CONCLUSIONS

The results of our studies present a new stage in solving the problem of the development of protective coatings of multicomponent and multielement systems, whose structural and phase characteristics make it possible to improve functional characteristics of various products that operate at high temperatures, loads, and wear rate, of cutting tools in particular.

It has been found that in the course of the deposition of the above systems there forms a three-phase structure with cubic, hexagonal, and tetragonal crystal lattices.

The hardness of the produced (Zr–Ti–Cr–Nb)N coatings has been found to change depending on the conditions of a material deposition and the resultant structural and phase compositions. The maximum hardness has been revealed of coatings with the largest crystallites that were produced at high nitrogen pressure in the chamber and substrate voltage. In the deposition of a coating with the maximum ($H = 43.7$ GPa) hardness the pulse stimulation has been used. The indentation load responsible for the formation of stresses exceeding the coating cohesion strength was $L_c = 62.06$ N.

The study was performed in the framework of two complex state budgetary programs The development of the principles of the formation of superhard nanostructural multicomponent coatings with high physicomechanical properties (number 0112U001382) and Physical principles of the plasma technology for a complex machining of multicomponent materials and coatings (number 0113U000137c).

REFERENCE

1. Azarenkov, N.A., Beresnev, V.M., Pogrebnjak, A.D., and Kolesnikov, D.A., *Nanostructurnye pokrytiya i nanomaterialy. Osnovy polucheniya. Svoistva. Oblasti primeneniya. Osobennosti sovremennogo nanostrukturnogo napravleniya v nanotekhnologii* (Nanostructural coatings and nanomaterials. Principles of production. Properties. Fields of applications. Special features of the modern nanostructural line in nanotechnology), Moscow: Librokom Book house, 2012.
2. Pogrebnjak, A.D., Shpak, A.P., Azarenkov, N.A., and Beresnev, V.M., Structures and properties of hard and superhard nanocomposite coatings, *Phys. Usp.*, 2009, vol. 52, no. 1, pp. 29–54.
3. Aouadi, S.M., Wong, K.C., Mitchell, K.A.R., Namavar, F., Tobin, E., Mihut, D.M., and Rohde, S.L., Characterization of titanium chromium nitride nanocomposite protective coatings, *Appl. Surf. Sci.*, 2004, vol. 229, nos. 1–4, pp. 387–394.
4. Han, J.G., Myung, H.S., Lee, H.M., and Shaginyan, L.R., Microstructure and mechanical properties of Ti–Ag–N and Ti–Cr–N superhard nanostructured coatings, *Surf. Coat. Technol.*, 2003, vols. 174–175, pp. 738–743.
5. Belov, D.S., Volkhonsky, A.O., Blinkov, I.V., et al., Multilayer nanostructured wear-resistant coatings with increased thermal stability, adapted to varying friction conditions, *Proc. Int. Conf. Nanomaterials: Applications and Properties*, 2013, vol. 2, no. 2, art. 02FNC10.
6. Boxman, R.L., Zhitomirsky, V.N., Grimberg, I., Rapoport, L., Goldsmith, S., and Weiss, B.Z., Structure and hardness of vacuum-arc deposited multi-component nitride coatings of Ti, Zr and Nb, *Surf. Coat. Technol.*, 2000, vol. 125, nos. 1–3, pp. 257–262.
7. Kim GwangSeok, Kim BomSok, Lee SangYul, and Hahn JunHee, Structure and mechanical properties of Cr–Zr–N films synthesized by closed field unbalanced magnetron sputtering with vertical magnetron sources, *Ibid.*, 2005, vol. 200, nos. 5–6, pp. 1669–1675.
8. Zhang, S., Wang, N., Li, D.J., Dong, L., Gu, H.Q., Wan, R.X., and Sun, X., The synthesis of Zr–Nb–N nanocomposite coating prepared by multitarget magnetron co-sputtering, *Nuclear Instruments and Methods in Physics Research Section B: Beam Interactions with Materials and Atoms*, 2013, vol. 307, pp. 119–122.
9. Pogrebnjak, A.D., Danilionok, M.M., Uglov, V.V., Erdybaeva, N.K., Kirik, G.V., Dub S.N., Rusakov, V.S., Shypylenko, A.P., Zukovski, P.V., and Tuleushev, Y.Zh., Nanocomposite protective coatings based on Ti–N–Cr/Ni–Cr–B–Si–Fe, their structure and properties, *Vacuum*, 2009, vol. 83, (SUPPL., 1), pp. S235–S239.
10. Musil, J., Hard nanocomposite coatings: Thermal stability, oxidation resistance and toughness, *Surf. Coat. Technol.*, 2012, vol. 207, pp. 50–65.
11. Hasegawa, H., Kimura, A., and Suzuki, T., Microhardness and structural analysis of (Ti,Al)N, (Ti,Cr)N, (Ti,Zr)N and (Ti,V)N films, *J. Vac. Sci. Technol. A*, 2000, vol. 18, no. 3, pp. 1038–1040.
12. Lee, J.-W., Chang, Sh.-T., Chen, H.-W., Chien, Ch.-H., Duh, J.-G., and Wang, Ch.-J., Microstructure, mechanical and electrochemical properties evaluation of pulsed DC reactive magnetron sputtered nanostructured Cr–Zr–N and Cr–Zr–Si–N thin films, *Surf. Coat. Technol.*, 2010, vol. 205, no. 5, pp. 1331–1338.
13. Pogrebnjak, A.D., Yakushchenko, I.V., Abadias, G., Chartier, P., Bondar, O.V., Beresnev, V.M., Takeda, Y., Sobol',O.V., Oyoshi, K., Andreyev, A.A., and Mukushev, B.A., The effect of the deposition parameters of nitrides of high-entropy alloys (Ti–Zr–Hf–V–Nb)N on their structure, composition, mechanical and tribological properties, *J. Superhard Mater.*, 2013, vol. 35, no. 6, pp. 356–368.
14. Belous, V.A., V'yugov, P.N., Kuprin, A.S., Leonov, S.A., Nosova, G.I., Ovcharenko, V.D., Ozhigov, L.S., Rudenko, A.G., Savchenko, V.I., Tolmacheva, G.N., and Khoroshikh, V.M., Mechanical characteristics of fuel element tubes from the Zr1Nb alloy after the deposition of ion–plasma coatings, *Problems Atom. Sci. Technol.*, 2013, vol. 2, no. 84, pp. 140–143.
15. Cokolenko, B.I., Mats, A.V., and Mats, V.A., Mechanical characteristics of zirconium and zirconium–niobium alloys, *High Pressure Physics and Technics*, 2013, vol. 23, no. 2, pp. 96–102.

16. Sobol', O.V., Pogrebnjak, A.D., and Beresnev, V.M., Effect of the manufacturing conditions on the phase composition, structure, and mechanical characteristics of vacuum-arc coatings of the Zr–Ti–Si–N system, *Physics of Metals and Metallography*, 2011, vol. 112, no. 2, pp. 199–206.

17. Slokar, L., Matkoviæ, T., and Matkoviæ, P., Alloy design and property evaluation of new Ti–Cr–Nb alloys, *Mater. Design*, 2012, vol. 33, pp. 26–30.

18. Beresnev, V.M., Sobol', O.V., Pogrebnjak, A.D., Turbin, P.V., and Litovchenko, S.V., Thermal stability of the phase composition, structure, and stressed state of ion-plasma condensates in the Zr–Ti–Si–N system, *Techn. Phys.*, 2010, vol. 55, no. 6, pp. 871–873.

19. Tsau, Ch.-H. and Chang, Yu-H., Microstructures and mechanical properties of $TiCrZrNbN_x$ alloy nitride thin films, *Entropy*, 2013, vol. 15, no. 11, pp. 5012–5021.

20. Pogrebnjak, A.D., Beresnev, V.M., Bondar, O.V., Abadias, G., Chartier, P., Postol'nyi, B.A., Andreev, A.A., and Sobol', O.V., The effect of nanolayer thickness on the structure and properties of multilayer TiN/MoN coatings, *Techn. Phys. Lett.*, 2014, vol. 40, no. 3, pp. 215–218.

21. Pogrebnjak, A.D., Shpak, A.P., Beresnev, V.M., Kolesnikov, D.A., Kunitskii, Yu.A., Sobol, O.V., Uglov, V.V., Komarov, F.F., Shypylenko, A.P., Makhmudov, N.A., Demyanenko, A.A., Baidak, V.S. , and Grudnitskii, V.V., Effect of thermal annealing in vacuum and in air on nanograin sizes in hard and superhard coatings Zr–Ti–Si–N, *J. Nanosci. Nanotechnol.*, 2012, vol. 12, no. 12, pp. 9213–9219.

22. Krause-Rehberg, R., Pogrebnyak, A.D., Borisyuk, V.N., Kaverin, M.V., Ponomarev, A.G., Bilokur, M.A., Oyoshi, K., Takeda, Y., Beresnev, V.M., and Sobol', O.V., Analysis of local regions near interfaces in nanostructured multicomponent (Ti–Zr–Hf–V–Nb)N coatings produced by the cathodic-arc–vapour deposition from an arc of an evaporating cathode, *Phys. Metals Metallography*, 2013, vol. 114, no. 8, pp. 672–680.

23. Pogrebnjak, A.D., Beresnev, V.M., Kolesnikov, D.A., Bondar, O.V., Takeda, Y., Oyoshi, K., Kaverin, V., Sobol, O.V., Krause-Rehberg, R., and Karwat, C., Multicomponent (Ti–Zr–Hf–V–Nb)N nanostructure coatings fabrication, high hardness and wear resistance, *Acta Physica Polonica A,* 2013, vol. 123, no. 5, pp. 816–818.

24. Pogrebnjak, A.D., Structure and properties of nanostructured (Ti–Hf–Zr–V–Nb)N coatings, *J. Nanomater.*, 2013, vol. 2013, art. ID 780125.

25. Umanskii, L.S., Skakov, Yu.S., Ivanov, A.S., and Rastorguev, L.N., *Kristallografiya, rentgenografiya i electronnaya microscopiya* (Crystallography, roentgenography and electron microscopy), Moscow: Metallurgiya, 1982.

26. Pogrebnjak, A.D. and Beresnev, V.M., *Nanocoatings Nanosystems Nanotechnologies*, Oak Park, IL: Bentham Sci. Publ., 2012.

27. Ivashchenko, V., Veprek, S., Pogrebnjak, A., and Postolnyi, B., First-principles quantum molecular dynamics study of $Ti_xZr_{1x}N(111)/SiN_y$ heterostructures and comparison with experimental results, *Sci. Technol. Adv. Mater.*, 2014, vol. 15, art. 025007.

Translated by G. Kostenchuk